electronic materials

MDPI

Article

Preparation of Li_3PS_4–Li_3PO_4 Solid Electrolytes by Liquid-Phase Shaking for All-Solid-State Batteries

Nguyen H. H. Phuc *, Takaki Maeda, Tokoharu Yamamoto, Hiroyuki Muto and Atsunori Matsuda *

Department of Electrical and Electronic Information Engineering, Toyohashi University of Technology, 1-1 Hibarigaoka, Tempaku, Toyohashi, Aichi 441-8580, Japan; maeda.takaki.px@tut.jp (T.M.); tktut2@gmail.com (T.Y.); muto@ee.edu.tut.ac.jp (H.M.)

* Correspondence: nguyen.huu.huy.phuc.hr@tut.jp (N.H.H.P.); matsuda@ee.tut.ac.jp (A.M.); Tel.: +81-532-44-6800 (A.M.); Fax: +81-532-48-583 (A.M.)

Abstract: A solid solution of a $100Li_3PS_4 \cdot xLi_3PO_4$ solid electrolyte was easily prepared by liquid-phase synthesis. Instead of the conventional solid-state synthesis methods, ethyl propionate was used as the reaction medium. The initial stage of the reaction among Li_2S, P_2S_5 and Li_3PO_4 was proved by ultraviolet-visible spectroscopy. The powder X-ray diffraction (XRD) results showed that the solid solution was formed up to $x = 6$. At $x = 20$, XRD peaks of Li_3PO_4 were detected in the prepared sample after heat treatment at 170 °C. However, the samples obtained at room temperature showed no evidence of Li_3PO_4 remaining for $x = 20$. Solid phosphorus-31 magic angle spinning nuclear magnetic resonance spectroscopy results proved the formation of a POS_3^{3-} unit in the sample with $x = 6$. Improvements of ionic conductivity at room temperature and activation energy were obtained with the formation of the solid solution. The sample with $x = 6$ exhibited a better stability against Li metal than that with $x = 0$. The all-solid-state half-cell employing the sample with $x = 6$ at the positive electrode exhibited a better charge–discharge capacity than that employing the sample with $x = 0$.

Keywords: liquid-phase synthesis; solid state electrolytes; all-solid-state battery; UV-Vis

Citation: Phuc, N.H.H.; Maeda, T.; Yamamoto, T.; Muto, H.; Matsuda, A. Preparation of Li_3PS_4–Li_3PO_4 Solid Electrolytes by Liquid-Phase Shaking for All-Solid-State Batteries. *Electron. Mater.* **2021**, *2*, 39–48. https://doi.org/10.3390/electronicmat2010004

Received: 2 February 2021
Accepted: 6 March 2021
Published: 12 March 2021

1. Introduction

Li_3PS_4 is one of the most important substances in the fields of sulfide-based solid electrolytes and all-solid-state batteries because of its ease of preparation and application. In general, Li_3PS_4 has three different crystal structures and an amorphous (glass) state [1,2]. The ionic conductivity and air stability of Li_3PS_4 can also be easily tuned by the addition of different materials, i.e., oxides, nitrides and halogens. The addition of an appropriate amount of LiI into the Li_3PS_4 structure is known to boost its ionic conductivity from approximately 5.0×10^{-4} S cm^{-1} to 6.5×10^{-4} S cm^{-1} [3,4]. Ambient air stability or suppression of H_2S evolution is also improved with the existence of LiI, CuO or FeS in a Li_3PS_4 glassy electrolyte [5,6].

Among the three crystal structures of α, β and γ for Li_3PS_4, the β phase has been reported to be only stable at temperatures higher than 160 °C [1]. Owing to its high ionic conductivity, the stabilization of the β phase at room temperature has been attracting efforts from researchers for years. One of the first attempts was made by Takada et al., who employed a melt quenching method to freeze this high-temperature phase and made it stable at room temperature [7]. The β phase was found to be easily synthesized at room temperature by the reaction between Li_2S and P_2S_5 in tetrahydrofuran (THF) [8]. The Li_3PS_4 glass-ceramic crystallized from $75Li_2S \cdot 25P_2S_5$ glass also showed the structure of the β phase [9,10].

The synthesis of Li_3PS_4 using liquid-phase synthesis with organic solvents as reaction media has been intensively investigated recently as an alternate chemical route for the preparation of sulfide-based solid electrolytes rather than the conventional solid state reaction [11–16]. In most of the reports, the effect of the solvents on the formation of Li_3PS_4

was of primary interest [17–21]. Many other types of organic solvents have been reported to be effective in promoting the reaction between Li_2S and P_2S_5, including tetrahydrofuran (THF), acetonitrile, ethyl acetate and ethyl propionate (EP). Furthermore, Li_3PS_4, $Li_7P_3S_{11}$ and argyrodite-type $Li_{7-y}PS_{6-y}X$ (X = Cl, Br and I) have also been reported to be obtained by the liquid-phase route. The formation of $Li_7P_3S_{11}$ was reported to be strongly dependent on the solvent structure. Dimethoxyethane and acetonitrile were the only two solvents that could promote the formation of $Li_7P_3S_{11}$ [22,23]. The preparation of argyrodite-type solid electrolytes usually requires a two-step process: Li_3PS_4 is first prepared by either a solid-state or liquid reaction, which is followed by the use of ethanol to dissolve all the components of the desired solid electrolytes [24–27].

The number of methods to improve the ionic conductivity of solid electrolytes prepared by the liquid-phase synthesis route is very limited; these methods include the addition of LiX (X = Cl, Br and I) and a thermal treatment procedure in the case of argyrodite-type solid electrolytes [28–32]. Doping Li_3PS_4 with oxygen ($75Li_2S{\cdot}23P_2S_5{\cdot}2P_2O_5$) resulted in the increase of ionic conductivity at room temperature (RT) from 1.83×10^{-4} Scm^{-1} to 2.53×10^{-4} Scm^{-1} [33]. However, Li_3PO_4 has been employed as a common additive to improve the ionic conductivity and electrochemical property of sulfide-based solid electrolytes [7,34–36]. In this study, $100Li_3PS_4{\cdot}xLi_3PO_4$ solid electrolytes were prepared by liquid-phase synthesis using ethyl propionate (EP). EP was employed in this study since it was suitable for Li_3PS_4 and Li_3PS_4—LiI solid electrolytes preparation [19,30]. Ultraviolet-visible (UV-Vis) spectroscopy evidenced the solvation of P_2S_5 but not of Li_3PO_4 in EP. The reaction between P_2S_5 and Li_3PO_4 in EP was also detected by UV-Vis spectroscopy. Solid phosphorus-31 magic angle spinning nuclear magnetic resonance (^{31}P MAS NMR) also revealed the formation of $POS_3{}^{3-}$, which confirmed the results from UV-Vis spectroscopy. An increase in ionic conductivity and decrease in activation energy were achieved by the addition of Li_3PO_4. An improvement of the stability against Li metal was also observed using the direct current polarization test. Better charge–discharge capacity of the all-solid-state (ASS) half-cell was also observed employing the sample with $x = 6$ compared with that employing the sample with $x = 0$.

2. Materials and Methods

Li_2S (99.9%, Mitsuwa, Torrance, CA, USA), P_2S_5 (99%, Merck, Kenilworth, NJ, USA) and Li_3PO_4 (99.99%, Aldrich, St. Louis, MO, USA) were purchased and used without any further treatment process. Super dehydrated ethyl propionate (EP) (99.5%, Aldrich) was dried again using a 3-Å molecular sieve for at least 24 h prior to usage. The positive electrode material, $LiNbO_3$-coated $LiNi_{1/3}Mn_{1/3}Co_{1/3}O_2$, was kindly donated by Toda Kogyo.

Li_2S, P_2S_5, Li_3PO_4 and P_2S_5–Li_3PO_4 were put into a screw vial followed by the addition of EP. The three bins were sealed in an Ar-filled glovebox and then ultrasonically treated for 30 min. The as-prepared samples were then filtered for UV-Vis measurement.

$100Li_3PS_4{\cdot}xLi_3PO_4$ solid electrolytes in this study were prepared from raw materials using the liquid-phase shaking method that has previously been reported [19]. Li_2S, P_2S_5 and Li_3PO_4 to form 1 g of $100Li_3PS_4$–xLi_3PO_4 were weighted and put into a plastic centrifuge tube together with zirconia balls (4 mm, 150 balls). The tube was filled with 20 mL of EP and then shaken at 1500 rpm for 6 h with amplitude of 1 cm. The received suspension was centrifuged and decanted to receive the precipitated pastes. The thus obtained samples were then dried under vacuum at room temperature and heat treated at 170 °C for 2 h.

The crystal structures of the samples were examined by X-ray diffraction (XRD; Ultima IV, Rigaku, Tokyo, Japan) using an air-tight holder to protect the samples from air humidity. Local structure of the prepared solid electrolytes was investigated by solid-state ^{31}P MAS NMR spectroscopy (Avance III 400, Bruker, Tokyo, Japan) using the typical single pulse sequence with a spinning rate of 5 kHz. UV-Vis spectra were recorded using a V-670 spectrophotometer (Jasco, Tokyo, Japan).

Alternating-current impedance spectroscopy (SI 1260, Solartron, Tokyo, Japan) was employed to measure the temperature dependence of the total conductivity of the prepared samples. Powder samples were placed in an PEEK holder (10 mm in diameter) with two SUS electrodes (Misumi) then pressed at 550 MPa (RT). The cell was placed under an Ar stream in a glass tube to measure the temperature dependence of resistivity. The temperature was gradually increased from room temperature to 210 °C and held at each temperature for 1 h prior to the impedance measurement.

The pelletized sample (diameter of 10 mm) with lithium metal sheets attached on both sides to serve as nonblocking electrodes were made to study the stability of solid electrolytes against lithium metal by DC polarization examination. Current collectors were Au-sputtered SUS rods. The cells were then cycled at ± 0.05 mA cm^{-2} under a dry Ar atmosphere using a charge-discharge device (NAGANO BST-2004H, Nagano, Japan).

An ASS half-cell was fabricated to investigate the electrochemical performance of the prepared solid electrolytes (SE). The prepared SE was employed as a separator and an In–Li alloy was used as the negative electrode. The positive electrode composites (PE) composed of $LiNbO_3$-coated $LiNi_{1/3}Mn_{1/3}Co_{1/3}O_2$ (NMC), solid electrolytes and acetylene black (weight ratio of 70:30:3) were prepared using agate mortar and pestle. The bilayer pellets (ϕ10 mm), composed of PE and separator layers (80 mg), were prepared by uniaxial pressing at 550 MPa. Indium foil was then attached onto the pellets by pressing at 200 MPa. The loading of PE in each cell was about 15 mg, in according to loading of NMC of 11–13 mg. Two stainless steel rods served as current collectors. Cyclic voltammetry (at RT) at a scan rate of 0.1 mV s^{-1} (SI1287 potentiostat, Solartron, Tokyo, Japan) was employed to study the electrochemical compatibility of the obtained SEs. The cells were cycled using a charge–discharge device (NAGANO BST-2004H, Nagano, Japan) in a dry Ar atmosphere. The cutoff voltages were in the range of 3.7–2.0 V vs. Li–In at 0.1 C. All the cells were placed in an insulation box that was kept at 30 $\pm$ 2 °C for 4 h prior to being tested. Cell preparation was conducted inside an Ar-filled glove-box with $O_2 \leq 1.0$ ppm and $H_2O \leq 0.1$ ppm.

3. Results

Figure 1 shows the optical images of the Li_2S, Li_3PO_4, P_2S_5 and Li_3PO_4–P_2S_5 solutions in EP solvent and UV-Vis spectra of the Li_3PO_4, P_2S_5 and Li_3PO_4–P_2S_5 solutions in EP solvent. The spectrum of the Li_3PO_4 solution exhibited no absorbance peak in the measurement range from 190 to 1200 nm. This result illustrated that Li_3PO_4 was unable to be dissolved in the EP solvent. The P_2S_5 solution had one sharp peak centered at approximately 264 nm, which indicated the dissolution of P_2S_5 in EP. The spectrum of Li_3PO_4–P_2S_5 in EP exhibited a large shoulder shape that was then deconvoluted into three other peaks centered at 264, 280 and 359 nm (small inset in Figure 1). The peak at 264 nm indicated the existence of P_2S_5 in the solution. The other two peaks originated from neither Li_3PO_4 nor P_2S_5, so they were proposed to arise from the products of the reaction between P_2S_5 and Li_3PO_4. The UV-Vis spectra proved that P_2S_5 dissolution in EP was the initial step for the reaction with Li_3PO_4 in EP solvent. To the best of our knowledge, this is the first time that such a reaction has been reported and evidenced using simple UV-Vis spectroscopy.

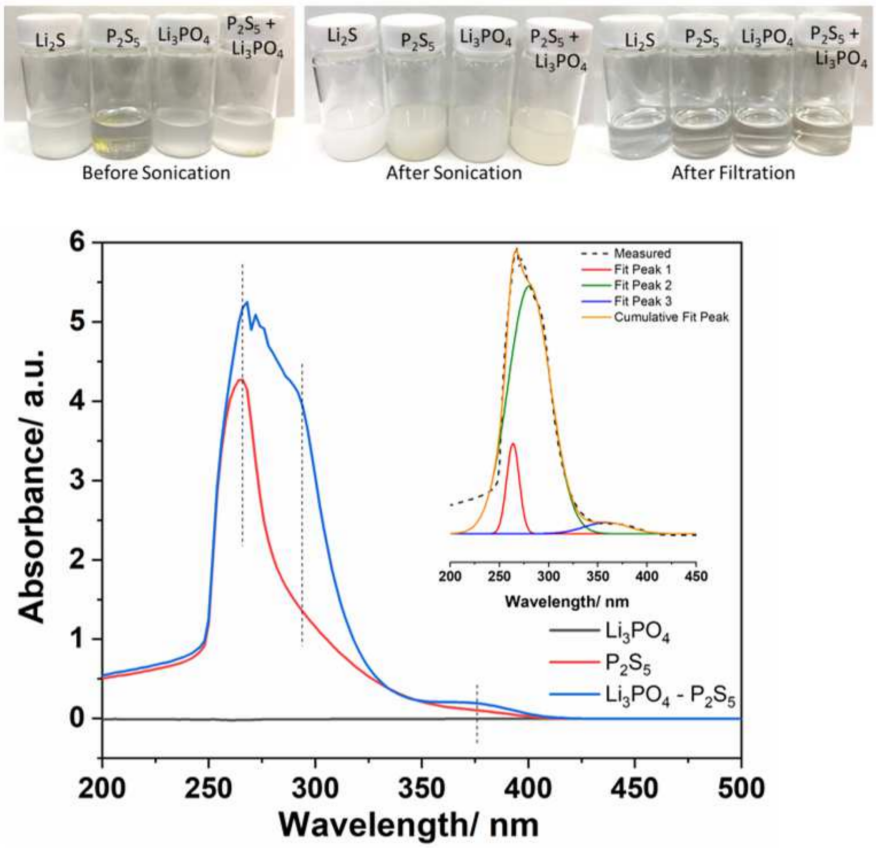

Figure 1. Optical photographs and UV-Vis spectra of Li_3PO_4, P_2S_5 and Li_3PO_4–P_2S_5 in EP solutions.

Figure 2 shows the XRD patterns of $100Li_3PS_4 \cdot xLi_3PO_4$ obtained after solvent elimination at room temperature (Figure 2a) and at 170 °C for 2 h (Figure 2b). The powder samples obtained at room temperature exhibited similar XRD patterns without any peak from the starting materials with a value of x of up to 20. The pattern resembled that of a cocrystal of Li_3PS_4 and EP that has been reported previously [19]. After solvent elimination at 170 °C, the XRD patterns of the retrieved samples exhibited the feature of β-Li_3PS_4, and signals of Li_3PO_4 (LPO) were also detected for the sample with x = 20 [8,18]. The XRD results proved that Li_3PO_4 could be incorporated into Li_3PS_4 up to at least 6 mol% by the proposed liquid-phase synthesis. As mentioned above, a solid solution between Li_3PS_4 and Li_3PO_4 was successfully prepared by the melt quenching method with x up to 50 but the structure of Li_3PS_4 was changed upon interaction with Li_3PO_4 [7]. Li_3PO_4 was doped into $0.6Li_2S \cdot 0.4SiS_2$ glass and glass-ceramic. It was observed that the $0.6Li_2S \cdot 0.4SiS_2$ glass could dissolve 20 mol% of Li_3PO_4 but its crystal structure was detected by XRD in the $0.6Li_2S \cdot 0.4SiS_2$ glass-ceramic [37]. Li_3PO_4 was also doped into the $70Li_2S \cdot 30P_2S_5$ glass-ceramic and was found to change the crystal structure from $Li_7P_3S_{11}$ to thio-LISICON II with only 5 mol% of dopant [38].

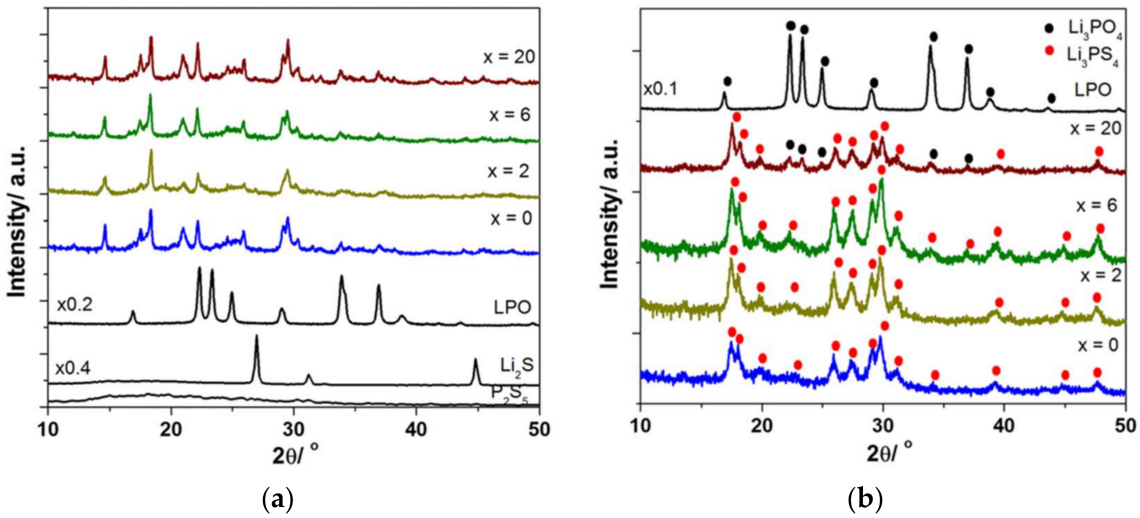

Figure 2. XRD patterns of $100Li_3PS_4$–xLi_3PO_4 samples dried at room temperature (RT) (**a**) and 170 °C (**b**).

Figure 3 shows the solid ^{31}P MAS NMR results of Li_3PO_4 and the samples with $x = 0$ and 6 (Figure 3a) and their deconvolution results (Figure 3b,c). The sample with $x = 6$ had a small peak located at 8.0 ppm that indicated the existence of Li_3PO_4, which resembled that of pristine Li_3PO_4. The large shoulder observed for the sample with $x = 0$ was composed of three other peaks located at 81.5, 83.6 and 85.7 ppm (Figure 3b). The peak located at 81.5 ppm was assigned to amorphous PS_4^{3-} [39,40]. The peaks at 83.6 and 85.7 were from PS_4^{3-} in β- and γ-Li_3PS_4, respectively [40]. Surprisingly, the area fraction of the amorphous phase was the highest, approximately 78%, while that of the β phase was just 15%. The main peak in the NMR spectrum of the sample with $x = 6$ was also decomposed into three peaks located at 82.4, 83.5 and 85.8 ppm (Figure 3c). The peaks at 82.4 and 85.8 originated from amorphous and crystal PS_4^{3-}. The peak at 83.5 ppm arose from both PS_4^{3-} and POS_3^{3-} ions [37]. In addition, the area fraction of the amorphous peak for the sample with $x = 6$ was 62% and that of the peak at 83.5 ppm was 32%. These values showed the reverse trend to that observed for the sample with $x = 0$ but the area fraction of PS_4^{3-} from γ-Li_3PS_4 was almost unchanged. These results proved the formation of a POS_3^{3-} ion and thus evidenced the reaction between P_2S_5 and Li_3PO_4 in an EP medium. The area fraction of the amorphous phase in the NMR spectra was surprisingly high in this study, which might be the reason for the low intensity of the XRD peak shown in Figure 2b.

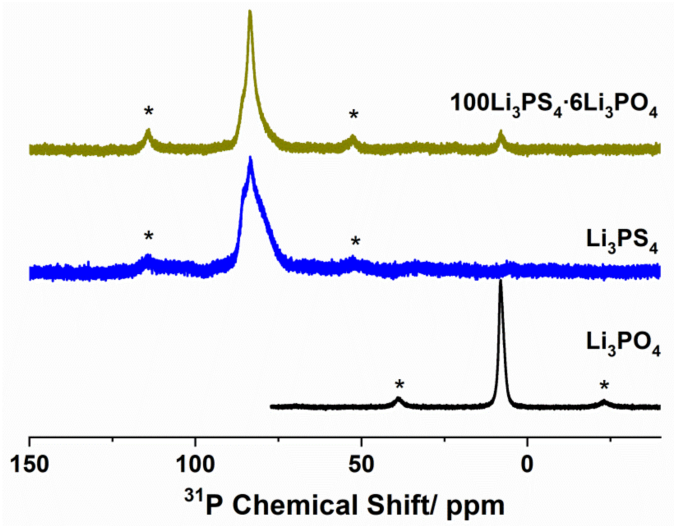

(**a**)

Figure 3. *Cont.*

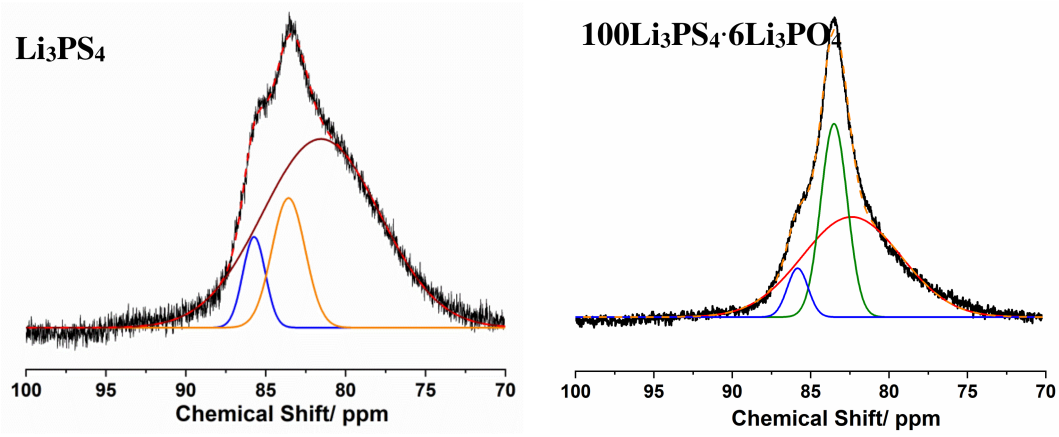

(**b**) (**c**)

Figure 3. ^{31}P Solid MAS NMR spectra of Li_3PO_4, Li_3PS_4 and $100Li_3PS_4{\cdot}6Li_3PO_4$ (**a**), the asterik * indicated the spinning side bands; deconvolution of main peak of Li_3PS_4 (**b**); deconvolution of main peak of $100Li_3PS_4{\cdot}6Li_3PO_4$ (**c**).

Figure 4 shows the temperature dependence of the ionic conductivity (Figure 4a) and conductivity at room temperature and activation energy as a function of x (Figure 4b) for $100Li_3PS_4{\cdot}xLi_3PO_4$. The temperature dependence of the ionic conductivity showed that at a temperature higher than 60 °C, the sample with $x = 0$ exhibited the highest ionic conductivity but below this temperature, the sample with $x = 6$ had the highest ionic conductivity. Conductivity at room temperature and activation energy as a function of x showed that upon addition of Li_3PO_4, the ionic conductivity started to increase and reached the highest value at $x = 6$. The activation energy showed the reverse trend with the ionic conductivity and reached the lowest value at $x = 6$. For the samples with $x = 0$ and 6, conductivity at room temperature was 1.9×10^{-4} and 3.3×10^{-4} Scm^{-1}, respectively, and activation energy was 42 and 27 kJ mol^{-1}, respectively. At x values higher than 6, the ionic conductivity started to reduce together with the increase in activation energy due to the remaining of Li_3PO_4 in the samples. The ionic conductivity of the samples obtained in this study was higher than the reported values of Li_3PS_4–Li_3PO_4 prepared by melt-quenching method but lower than the glass-ceramic samples [7,41]. Li ion movement changing from 2D to 3D with oxygen doping was the main reason for improvement in both ionic conductivity and activation energy of β-Li_3PS_4 as shown by Wang et al. in their DFT calculation study [42]. Oxygen doping in both glass and glass-ceramic Li_3PS_4 solid electrolytes was found to be an effective method to boot their ionic conductivity by using either Li_2O or P_2O_5 as oxygen sources [41,43].

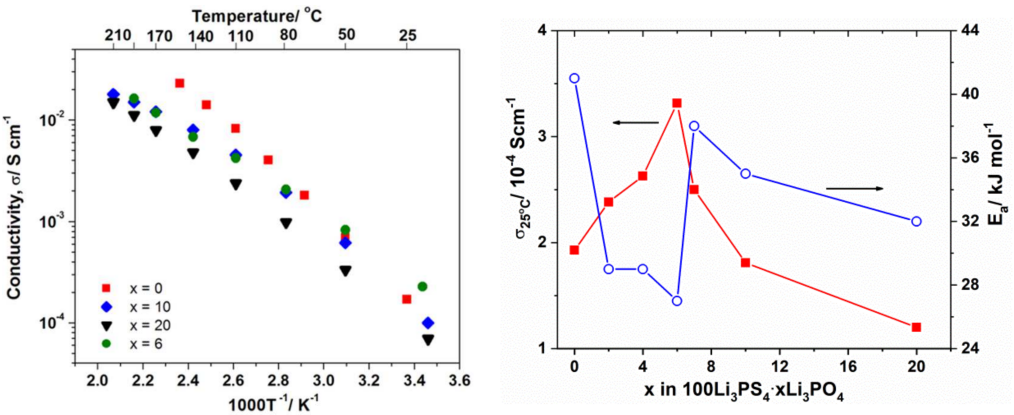

(**a**) (**b**)

Figure 4. Temperature dependence of conductivity of $100Li_3PS_4{\cdot}xLi_3PO_4$ samples dried at 170 °C; (**a**) room temperature ionic conductivity and (**b**) activation energy as a function of composition.

Two symmetric cells, Li | Li_3PS_4 | Li and Li | $100Li_3PS_4{\cdot}6Li_3PO_4$ | Li, were constructed to investigate the stability of the samples with $x = 0$ and 6 against Li metal using the direct current polarization test. The results are illustrated in Figure 5a. The Li | Li_3PS_4 | Li cell had an initial voltage of approximately 32 mV while that of the Li | $100Li_3PS_4{\cdot}6Li_3PO_4$ | Li cell was approximately 18 mV because of the smaller resistivity. The Li | Li_3PS_4 | Li cell exhibited a slight change of its voltage to approximately 35 mV after 100 h in the test condition. In contrast, the Li | $100Li_3PS_4{\cdot}6Li_3PO_4$ | Li cell exhibited a voltage profile that was nearly constant after 200 h in the working condition. These results proved that the addition of Li_3PO_4 was able to improve the stability of sulfide-based solid electrolytes against metallic Li. A similar enhancement of the stability against metallic Li was obtained when β-Li_3PS_4 was doped with Sb_2O_5 [44]. The improvement of the stability against metallic Li was explained by the formation of an interfacial buffer layer from the reaction between solid electrolytes and metallic Li [45].

$LiNbO_3$-coated $LiNi_{1/3}Mn_{1/3}Co_{1/3}O_2$ instead of bare $LiNi_{1/3}Mn_{1/3}Co_{1/3}O_2$ was employed to reduce the side reaction occurring at the solid electrolyte and active material interface [45]. The initial charge capacities of both cells using the samples with $x = 0$ and $x = 6$ were 170 mAh $g^{-1}{}_{NMC}$, respectively, and the discharge capacities were 148 and 150 mAh $g^{-1}{}_{NMC}$, respectively. From the second cycle, the discharge capacity of the cell for the sample with $x = 6$ increased to 158 mAh $g^{-1}{}_{NMC}$ whereas that of the sample with $x = 0$ reduced to 146 mAh $g^{-1}{}_{NMC}$. The superior discharge capacity of the cell employing the sample with $x = 6$, compared with that of the cell employing the sample with $x = 0$, remained for the investigated 20 cycles. These results proved that doping Li_3PS_4 with 6 mol% Li_3PO_4 improved the cell performance compared with the intrinsic electrolyte sample.

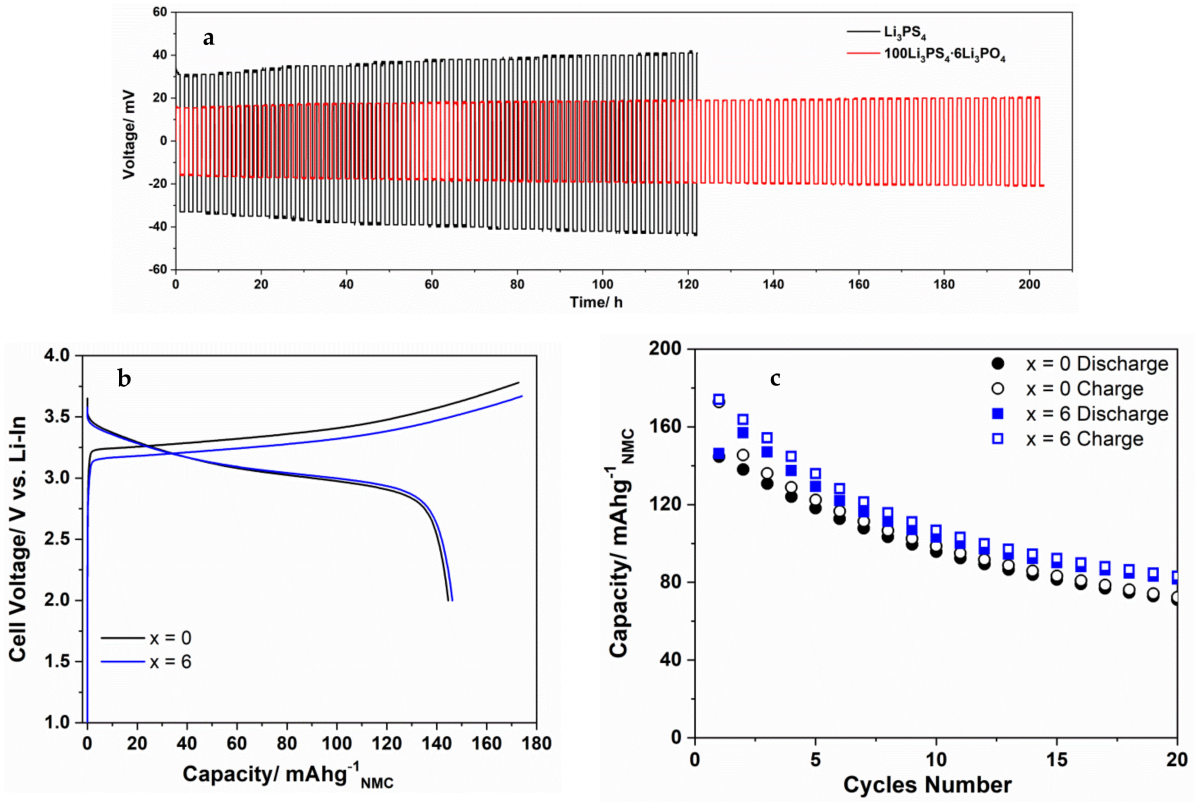

Figure 5. DC polarization of Li | LPSO | Li cell at 0.05 mA cm^{-2} (**a**); first charge–discharge curves and cyclic properties of all-solid-state cells employing either sample with $x = 0$ or 6 as solid electrolytes at the positive electrodes (**b**); cyclic performance of all-solid-state half-cells employing samples with $x = 0$ and $x = 6$ at the positive electrodes (**c**).

4. Conclusions

$100Li_3PS_4 \cdot xLi_3PO_4$ solid electrolytes were successfully prepared by the liquid-phase shaking method using EP as the reaction medium. The reaction between Li_3PO_4 and P_2S_5 was evidenced by UV-Vis spectroscopy, where the dissolution of P_2S_5 in EP was the initial step of the activation of Li_3PO_4. The formation of the $POS_3{}^{3-}$ ion was further proved by solid ^{31}P MAS NMR. It was observed that the incorporation of Li_3PO_4 into Li_3PS_4 could improve not only the ionic conductivity and activation energy but also stability against metallic Li. The charge–discharge capacities of the all-solid-state cell employing the $100Li_3PS_4 \cdot 6Li_3PO_4$ solid electrolyte at the positive electrode was slightly higher than those of the cell using Li_3PS_4 in the positive electrode.

Author Contributions: Conceptualization, methodology, software, validation, formal analysis, N.H.H.P.; investigation, N.H.H.P., T.M. and T.Y.; writing—original draft preparation, N.H.H.P.; writing—review and editing, N.H.H.P. and A.M.; supervision, A.M. and H.M.; project administration, A.M. and H.M.; funding acquisition, A.M. and H.M. All authors have read and agreed to the published version of the manuscript.

Funding: This study was supported by the Advanced Low Carbon Technology Specially Promoted Research for Innovative Next Generation Batteries (JST-ALCA-SPRING, Grant No. JPMJAL1301) program of the Japan Science and Technology Agency.

Institutional Review Board Statement: Not applicable.

Informed Consent Statement: Not applicable.

Data Availability Statement: The data presented in this study are available on request from the corresponding authors.

Acknowledgments: The authors appreciate R. Kato of the Cooperative Research Facility Center, Toyohashi University of Technology for his assistance in NMR measurement. We thank Edanz Group (https://en-author-services.edanzgroup.com/ac) for editing a draft of this manuscript.

Conflicts of Interest: The authors declare no conflict of interest. The funders had no role in the design of the study; in the collection, analyses, or interpretation of the data; in the writing of the manuscript, or in the decision to publish the results.

References

1. Homma, K.; Yonemura, M.; Kobayashi, T.; Nagao, M.; Hirayama, M.; Kanno, R. Crystal structure and phase transitions of the lithium ionic conductor Li_3PS_4. *Solid State Ion.* **2011**, *182*, 53–58. [CrossRef]
2. Muramatsu, H.; Hayashi, A.; Ohtomo, T.; Hama, S.; Tatsumisago, M. Tatsumisago, Structural change of Li_2S–P_2S_5 sulfide solid electrolytes in the atmosphere. *Solid State Ion.* **2011**, *182*, 116–119. [CrossRef]
3. Feng, X.; Chien, P.-H.; Patel, S.; Zheng, J.; Immediato-Scuotto, M.; Xin, Y.; Hung, I.; Gan, Z.; Hu, Y.-Y. Synthesis and characterizations of highly conductive and stable electrolyte $Li_{10}P_3S_{12}I$. *Energy Storage Mater.* **2019**, *22*, 397–401. [CrossRef]
4. Spannenberger, S.; Miß, V.; Klotz, E.; Kettner, J.; Cronau, M.; Ramanayagam, A.; Di Capua, F.; Elsayed, M.; Krause-Rehberg, R.; Vogel, M.; et al. Annealing-induced vacancy formation enables extraordinarily high Li+ ion conductivity in the amorphous electrolyte 0.33LiI + 0.67Li_3PS_4. *Solid State Ion.* **2019**, *341*. [CrossRef]
5. Ohtomo, T.; Hayashi, A.; Tatsumisago, M.; Kawamoto, K. Suppression of H_2S gas generation from the $75Li_2S \cdot 25P_2S_5$ glass electrolyte by additives. *J. Mater. Sci.* **2013**, *48*, 4137–4142. [CrossRef]
6. Calpa, M.; Rosero-Navarro, N.C.; Miura, A.; Jalem, R.; Tateyama, Y.; Tadanaga, K. Chemical stability of Li_4PS_4I solid electrolyte against hydrolysis. *Appl. Mater. Today* **2021**, *22*, 100918.
7. Takada, K.; Osada, M.; Ohta, N.; Inada, T.; Kajiyama, A.; Sasaki, H.; Kondo, S.; Watanabe, M.; Sasaki, T. Lithium ion conductive oxysulfide, Li_3PO_4–Li_3PS_4. *Solid State Ion.* **2005**, *176*, 2355–2359. [CrossRef]
8. Liu, Z.; Fu, W.; Payzant, E.A.; Yu, X.; Wu, Z.; Dudney, N.J.; Kiggans, J.; Hong, K.; Rondinone, A.J.; Liang, C. Anomalous high ionic conductivity of nanoporous beta-Li_3PS_4. *J. Am. Chem. Soc.* **2013**, *135*, 975–978. [CrossRef] [PubMed]
9. Tsukasaki, H.; Mori, S.; Morimoto, H.; Hayashi, A.; Tatsumisago, M. Direct observation of a non-crystalline state of Li_2S-P_2S_5 solid electrolytes. *Sci. Rep.* **2017**, *7*, 1–7. [CrossRef]
10. Tsukasaki, H.; Mori, S.; Shiotani, S.; Yamamura, H. Yamamura, Ionic conductivity and crystallization process in the Li_2S–P_2S_5 glass electrolyte. *Solid State Ion.* **2018**, *317*, 122–126. [CrossRef]
11. Ohara, K.; Masuda, N.; Yamaguchi, H.; Yao, A.; Tominaka, S.; Yamada, H.; Hiroi, S.; Takahashi, M.; Yamamoto, K.; Wakihara, T.; et al. Observation of Liquid Phase Synthesis of Sulfide Solid Electrolytes Using Time-Resolved Pair Distribution Function Analysis. *Phys. Status Solidi* **2020**, *257*, 2000106. [CrossRef]

12. Yamamoto, K.; Takahashi, M.; Ohara, K.; Phuc, N.H.H.; Yang, S.; Watanabe, T.; Uchiyama, T.; Sakuda, A.; Hayashi, A.; Tatsumisago, M.; et al. Synthesis of Sulfide Solid Electrolytes through the Liquid Phase: Optimization of the Preparation Conditions. *ACS Omega* **2020**, *5*, 26287–26294. [CrossRef]
13. Takahashi, M.; Yang, S.; Yamamoto, K.; Ohara, K.; Phuc, N.H.H.; Watanabe, T.; Uchiyama, T.; Sakuda, A.; Hayashi, A.; Tatsumisago, M.; et al. Improvement of lithium ionic conductivity of Li_3PS_4 through suppression of crystallization using low-boiling-point solvent in liquid-phase synthesis. *Solid State Ion.* **2021**, *361*, 115568. [CrossRef]
14. Calpa, M.; Rosero-Navarro, N.C.; Miura, A.; Terai, K.; Utsuno, F.; Tadanaga, K. Tadanaga, Formation Mechanism of Thiophosphate Anions in the Liquid-Phase Synthesis of Sulfide Solid Electrolytes Using Polar Aprotic Solvents. *Chem. Mater.* **2020**, *32*, 9627–9632. [CrossRef]
15. Ghidiu, M.; Schlem, R.; Zeier, W.G. Pyridine Complexes as Tailored Precursors for Rapid Synthesis of Thiophosphate Superionic Conductors. *Batter. Supercaps* **2020**. [CrossRef]
16. Maniwa, R.; Calpa, M.; Rosero-Navarro, N.C.; Miura, A.; Tadanaga, K. Synthesis of sulfide solid electrolytes from Li_2S and P_2S_5 in anisole. *J. Mater. Chem. A* **2021**, *9*, 400–405. [CrossRef]
17. Phuc, N.H.H.; Morikawa, K.; Totani, M.; Muto, H.; Matsuda, A. Chemical synthesis of Li_3PS_4 precursor suspension by liquid-phase shaking. *Solid State Ion.* **2016**, *285*, 2–5. [CrossRef]
18. Phuc, N.H.H.; Totani, M.; Morikawa, K.; Muto, H.; Matsuda, A. Preparation of Li_3PS_4 solid electrolyte using ethyl acetate as synthetic medium. *Solid State Ion.* **2016**, *288*, 240–243. [CrossRef]
19. Phuc, N.H.H.; Morikawa, K.; Mitsuhiro, T.; Muto, H.; Matsuda, A. Synthesis of plate-like Li_3PS_4 solid electrolyte via liquid-phase shaking for all-solid-state lithium batteries. *Ionics* **2017**, *23*, 2061–2067. [CrossRef]
20. Phuc, N.H.H.; Muto, H.; Matsuda, A. Fast preparation of Li_3PS_4 solid electrolyte using methyl propionate as synthesis medium. *Mater. Today Proc.* **2019**, *16*, 216–219. [CrossRef]
21. Wang, H.; Hood, Z.D.; Xia, Y.; Liang, C. Fabrication of ultrathin solid electrolyte membranes of β-Li_3PS_4 nanoflakes by evaporation-induced self-assembly for all-solid-state batteries. *J. Mater. Chem. A* **2016**, *4*, 8091–8096. [CrossRef]
22. Ito, S.; Nakakita, M.; Aihara, Y.; Uehara, T.; Machida, N. A synthesis of crystalline $Li_7P_3S_{11}$ solid electrolyte from 1,2-dimethoxyethane solvent. *J. Power Sources* **2014**, *271*, 342–345. [CrossRef]
23. Xu, R.; Xia, X.; Yao, Z.; Wang, X.; Gu, C.; Tu, J. Preparation of $Li_7P_3S_{11}$ glass-ceramic electrolyte by dissolution-evaporation method for all-solid-state lithium ion batteries. *Electrochim. Acta* **2016**, *219*, 235–240. [CrossRef]
24. Ziolkowska, D.A.; Arnold, W.; Druffel, T.; Sunkara, M.K.; Wang, H. Rapid and Economic Synthesis of a Li_7PS_6 Solid Electrolyte from a Liquid Approach. *ACS Appl. Mater. Interfaces* **2019**, *11*, 6015–6021. [CrossRef]
25. Yubuchi, S.; Uematsu, M.; Deguchi, M.; Hayashi, A.; Tatsumisago, M. Lithium-Ion-Conducting Argyrodite-Type Li_6PS_5X (X = Cl, Br, I) Solid Electrolytes Prepared by a Liquid-Phase Technique Using Ethanol as a Solvent. *ACS Appl. Energy Mater.* **2018**, *1*, 3622–3629. [CrossRef]
26. Zhou, L.; Park, K.-H.; Sun, X.; Lalère, F.; Adermann, T.; Hartmann, P.; Nazar, L.F. Solvent-Engineered Design of Argyrodite Li_6PS_5X (X = Cl, Br, I) Solid Electrolytes with High Ionic Conductivity. *ACS Energy Lett.* **2018**, *4*, 265–270. [CrossRef]
27. Chida, S.; Miura, A.; Rosero-Navarro, N.C.; Higuchi, M.; Phuc, N.H.; Muto, H.; Matsuda, A.; Tadanaga, K. Liquid-phase synthesis of Li_6PS_5Br using ultrasonication and application to cathode composite electrodes in all-solid-state batteries. *Ceram. Int.* **2018**, *44*, 742–746. [CrossRef]
28. Rangasamy, E.; Liu, Z.; Gobet, M.; Pilar, K.; Sahu, G.; Zhou, W.; Wu, H.; Greenbaum, S.; Liang, C. An iodide-based $Li_7P_2S_8I$ superionic conductor. *J. Am. Chem. Soc.* **2015**, *137*, 1384–1387. [CrossRef]
29. Phuc, N.H.H.; Hirahara, E.; Morikawa, K.; Muto, H.; Matsuda, A. One-pot liquid phase synthesis of $(100 - x)Li_3PS_4$—xLiI solid electrolytes. *J. Power Sources* **2017**, *365*, 7–11. [CrossRef]
30. Phuc, N.H.H.; Yamamoto, T.; Muto, H.; Matsuda, A. Fast synthesis of Li_2S–P_2S_5–LiI solid electrolyte precursors. *Inorg. Chem. Front.* **2017**, *4*, 1660–1664. [CrossRef]
31. Yamamoto, T.; Phuc, N.H.H.; Muto, H.; Matsuda, A. Preparation of $Li_7P_2S_8I$ Solid Electrolyte and Its Application in All-Solid-State Lithium-Ion Batteries with Graphite Anode. *Electron. Mater. Lett.* **2019**, *15*, 409–414. [CrossRef]
32. Arnold, W.; Buchberger, D.A.; Li, Y.; Sunkara, M.; Druffel, T.; Wang, H. Halide doping effect on solvent-synthesized lithium argyrodites Li_6PS_5X (X= Cl, Br, I) superionic conductors. *J. Power Sources* **2020**, *464*, 228158. [CrossRef]
33. Li, J.; Liu, W.; Zhang, X.; Ma, Y.; Wei, Y.; Fu, Z.; Li, J.; Yan, Y. Heat treatment effects in oxygen-doped β-Li_3PS_4 solid electrolyte prepared by wet chemistry method. *J. Solid State Electrochem.* **2021**, 1–11. [CrossRef]
34. Takada, K.; Aotani, N.; Kondo, S. Electrochemical behaviors of Li+ ion conductor, Li_3PO_4-Li_2S-SiS_2. *J. Power Sources* **1993**, *43–44*, 135–141. [CrossRef]
35. Nagamedianova, Z.; Hernández, A.; Sánchez, E. Conductivity studies on LiX–Li_2S–Sb_2S_3–P_2S_5 (X = LiI or Li_3PO_4) glassy system. *Ionics* **2006**, *12*, 315–322. [CrossRef]
36. Mo, S.; Lu, P.; Ding, F.; Xu, Z.; Liu, J.; Liu, X.; Xu, Q. High-temperature performance of all-solid-state battery assembled with $95(0.7Li_2S\text{-}0.3P_2S_5)\text{-}5Li_3PO_4$ glass electrolyte. *Solid State Ion.* **2016**, *296*, 37–41. [CrossRef]
37. Hayashi, K.T.A.; Tatsumisago, M.; Minami, T.; Miura, Y. Structural Change Accompanying Crystallization in the Lithium lon Conductive Li_2S-SiS_2-Li_3PO_4 Oxysulfide Glasses. *J. Ceram. Soc. Jpn.* **1999**, *107*, 510–516. [CrossRef]
38. Huang, B.; Yao, X.; Huang, Z.; Guan, Y.; Jin, Y.; Xu, X. Li_3PO_4 -doped $Li_7P_3S_{11}$ glass-ceramic electrolytes with enhanced lithium ion conductivities and application in all-solid-state batteries. *J. Power Sources* **2015**, *284*, 206–211. [CrossRef]

39. Eckert, Z.Z.H.; Kennedy, J.H. Structural Transformation of Non-Oxide Chalcogenide Glasses. The Short-Range Order of Li_2S-P_2S_5 Glasses Studied by Quantitative ^{31}P and ^{6,7}Li High-Resolution Solid-state NMR. *Chem. Mater.* **1990**, *2*, 273–279. [CrossRef]
40. Gobet, M.; Greenbaum, S.; Sahu, G.; Liang, C. Structural Evolution and Li Dynamics in Nanophase Li_3PS_4 by Solid-State and Pulsed-Field Gradient NMR. *Chem. Mater.* **2014**, *26*, 3558–3564. [CrossRef]
41. Tao, Y.; Chen, S.; Liu, D.; Peng, G.; Yao, X.; Xu, X. Lithium Superionic Conducting Oxysulfide Solid Electrolyte with Excellent Stability against Lithium Metal for All-Solid-State Cells. *J. Electrochem. Soc.* **2016**, *163*, A96–A101. [CrossRef]
42. Wang, R.X.X.; Li, H.; Chen, L. Oxygen-driven transition from two-dimensional to three-dimensional transport behavior in β-Li_3PS_4 electrolyte. *Phys. Chem. Chem. Phys.* **2016**, *18*, 21269–21277. [CrossRef] [PubMed]
43. Machida, N.; Yoneda, Y.; Shigematsu, T. Mechano-chemical Synthesis of Lithium Ion Conducting Materials in the System Li_20-Li_2S-P_2S_5. *J. Jpn. Soc. Powder Powder Metall.* **2004**, *51*, 91–97. [CrossRef]
44. Xie, D.; Chen, S.; Zhang, Z.; Ren, J.; Yao, L.; Wu, L.; Yao, X.; Xu, X. High ion conductive Sb_2O_5-doped β-Li_3PS_4 with excellent stability against Li for all-solid-state lithium batteries. *J. Power Sources* **2018**, *389*, 140–147. [CrossRef]
45. Zhu, Y.; He, X.; Mo, Y. Origin of Outstanding Stability in the Lithium Solid Electrolyte Materials: Insights from Thermodynamic Analyses Based on First-Principles Calculations. *ACS Appl. Mater. Interfaces* **2015**, *7*, 23685–23693. [CrossRef]